



Significantly enhanced dielectric properties and chain segmental dynamics of PEO/SnO₂ nanocomposites

Priyanka Dhatarwal¹ · Shobhna Choudhary² · R. J. Sengwa¹

Received: 4 November 2019 / Revised: 4 March 2020 / Accepted: 23 April 2020 / Published online: 2 May 2020
© Springer-Verlag GmbH Germany, part of Springer Nature 2020

Abstract

Poly(ethylene oxide) (PEO) matrix- and tin oxide (SnO₂) nanofiller-based polymer nanocomposite films were prepared by solution cast followed by melt press. The effect of SnO₂ concentration (i.e. 1, 3, and 5 wt%) on the structure, dielectric permittivity, and chain segmental motion of PEO was investigated with X-ray diffraction, Fourier transform infrared spectroscopy, scanning electron microscopy, and dielectric relaxation spectroscopy (DRS) techniques. Results reveal that the dispersion of SnO₂ nanoparticles has enormously altered the contents of different crystalline phases of the PEO and some amount of the degree of crystallinity. The DRS study in the range of 20 Hz–1 MHz at 30 °C confirmed that the complex dielectric permittivity and electrical conductivity at lower frequencies increased largely on the dispersion of SnO₂ nanoparticles in the PEO matrix which was attributed to the contribution of interfacial polarization effect, moreover, a significant increase was also noted in the molecular polarization at higher frequencies. The relaxation processes corresponding to Maxwell–Wagner–Sillars mechanism and PEO chain segmental motion were analysed from the electric modulus spectra. The chain segmental dynamics and dc electrical conductivity have nonlinearly enhanced with the increase in SnO₂ content in the polymer structure. The temperature-dependent dielectric and relaxation behaviour of PEO-3 wt% SnO₂ film was also reported. It was observed that the relaxation time and electrical conductivity of the film exhibited Arrhenius behaviour of low activation energies.

Keywords Polymer nanocomposite · Dielectric properties · Relaxation time · XRD · FTIR

✉ R. J. Sengwa
rjsengwa@rediffmail.com; rjs.ph@jnvu.edu.in

¹ Dielectric Research Laboratory, Department of Physics, Jai Narain Vyas University, Jodhpur 342 005, India

² CSIR – National Institute of Science Communication and Information Resources, New Delhi 110 012, India

Introduction

Polymer matrices dispersed with inorganic/organic nanomaterial-based flexible-type advanced materials prepared by state of the art are categorized as polymer nanocomposites (PNCs) [1]. Tunable dielectric and electrical properties of several PNC materials have accredited them as novel polymeric nanodielectrics (PNDs) for their multifunctional uses in the design and development of advanced microelectronic devices [2–12]. These PNDs simultaneously bear characteristic properties of the host polymer matrix and that of the inorganic nanofiller [2, 3, 9]. Therefore, the PNC and/or PND materials are well established as potential candidates for the advancement of numerous organoelectronic and optoelectronic devices [5–7, 13–18], high-performance memory devices [19], as ultraviolet and microwave shielders [9, 20], wideband microwave antennas development [21], fabrication of high-energy-density capacitors [4, 22], energy harvester [23], photocatalysis [24], gas sensor [25], solid polymer electrolytes for energy storage/converter devices [26–28], etc. In the last few decades, the dielectric and electrical characterization of PNC materials to recognize them as useful PNDs has been an intense field of researches [2–12, 16, 17, 25, 29, 30]. Several studies concluded that the interface of polymer structures with the bare and/or functionalized surface of inorganic nanofillers plays an important role in tailoring the promising properties of the PNDs including their dielectric behaviour over the broad frequency range [2, 3, 10, 12, 16, 20, 31–33].

In the past few years, extensive work on the dielectric and structural properties of numerous PNC materials for the confirmation of their applications as novel PNDs has been carried out in our laboratory [9, 10, 34–41]. These materials were prepared using polar polymers namely poly(ethylene oxide) (PEO), poly(vinyl alcohol) (PVA), poly(vinyl pyrrolidone) (PVP), poly(methyl methacrylate) (PMMA), poly(vinylidene fluoride) (PVDF), and also their blends with different inorganic nanofillers (i.e. montmorillonite (MMT) clay, silica (SiO_2), alumina (Al_2O_3), zinc oxide (ZnO), titanium dioxide (TiO_2), and tin oxide (SnO_2)). The SnO_2 is an important n-type semiconductor oxide having wide energy band gap (~ 3.6 eV) [42]. It is frequently used with different polymers for the preparation of transparent organic resistive memory devices, gas sensors, transparent electrodes for solar cells, electrochromic windows, and electrolytes for energy storage/converter devices [19, 23, 28, 41–44]. Furthermore, the SnO_2 nanoparticles dispersed PEO matrix has also been considered for the preparation of high-performance nanocomposite solid polymer electrolytes (NSPEs) as potential candidates for energy storage/converter devices [45, 46].

Survey of the literature unveils that the structural, dielectric, and electrical properties of SnO_2 -incorporated PEO matrix-based PNC films are yet to be characterized for their nanodielectric applications. In this manuscript, we report the detailed dielectric behaviour and relaxation processes of the PEO- x wt% SnO_2 films ($x=0, 1, 3$, and 5) over the frequency range from 20 Hz to 1 MHz, at ambient temperature, and also with the temperature variation for the PEO-3 wt% SnO_2 film. The alteration in the degree of crystallinity of the PEO matrix with

the variation of SnO₂ concentration and also the morphological changes of these materials have been studied. Further, the SnO₂ nanofiller concentration in these materials was kept low (≤ 5 wt%) in order to avoid the nanoparticles agglomeration for the successful preparation of the PNCs [2, 3, 9].

Experimental

Materials

PEO powder of $M_v = 600,000$ g/mol (CAS 25322-68-3) and SnO₂ nanopowder of particle sizes < 100 nm (CAS 18282-10-5) were purchased from Sigma-Aldrich, USA.

The PNC films of PEO matrix incorporated with x wt% SnO₂ with respect to the amount of PEO were prepared by the solution cast method followed by a melt press technique. Initially, 1 g amount of PEO for the preparation for each of the four samples was dissolved in 10 mL acetonitrile in separate glass bottles. The SnO₂ amounts 0.01, 0.03, and 0.05 g for x values 1, 3, and 5 wt%, respectively, were dispersed in 5 mL acetonitrile in separate glass bottles under magnetic stirring. Thereafter, one of the PEO solutions and 1 wt% SnO₂ dispersed solution were mixed and the mixture was firstly sonicated and subsequently magnetically stirred until a homogeneous viscous solution of polymeric nanocomposite was obtained. This solution was cast on to a polypropylene petri dish to dry at room temperature which resulted PEO-1 wt% SnO₂ film. The same steps were followed for the preparation of 3 and 5 wt% SnO₂-containing PNC films. The solution-casted PNC film was placed in circular stainless steel die of 50 mm diameter having fixed spacer, and then, it was heated up to PEO melting temperature (~ 70 °C) with the polymer press film-making unit. This melted composite material was pressed under 2 tons pressure per unit area, and then, the heater was turned off. This melt-pressed material was slowly cooled down to room temperature which resulted in a PNC film of uniform thickness and of equally smooth surfaces. All the solution-casted PNC films and the pristine PEO film ($x = 0$) were melt-pressed one by one following the same procedure. These solution-casted and melt-pressed PNC films of thickness ~ 0.42 mm were vacuum-dried prior to their structural and dielectric characterizations.

Characterizations

PANalytical X'pert Pro multipurpose X-ray powder diffractometer with monochromatized Cu-K α radiation (wavelength $\lambda = 0.15406$ nm) operated at 1800 W (45 kV and 40 mA) was used for recording diffractograms (X-ray diffraction (XRD) patterns) of the PEO- x wt% SnO₂ films. The diffraction data for each film were collected in the reflection mode over the 2θ range from 10° to 55° with a scan rate of $0.05^\circ/\text{s}$. An Agilent technologies Fourier transform infrared (FTIR) spectrometer (Cary 630) was used for collecting the FTIR spectra in ATR mode to confirm the polymer–nanoparticle interaction behaviour in these PNC materials. Carl ZEISS

EVO 18 scanning electron microscope (SEM) was used for taking the micrographs of surface and fractured cross section of the PNC films.

Agilent technologies 4284A precision LCR meter was used for performing the dielectric relaxation spectroscopy (DRS) of the PNC films over the frequency range of 20 Hz–1 MHz under 1 V applied electric field at 30 °C and also with the temperature variation from 30 to 60 °C for the PEO-3 wt% SnO₂ film. For carrying out the DRS of each PNC film, it was mounted in the Agilent technologies 16451B solid dielectric test fixture to make capacitive configuration of capacitance C_p , resistance R_p , and the dielectric loss tangent ($\tan\delta$). The dielectric test fixture was kept in a microprocessor-controlled oven for the measurements of the film at different temperatures. The complex permittivity, alternating current (ac) electrical conductivity, and electric modulus spectra of the PNC films were derived using frequency-dependent C_p , R_p , and $\tan\delta$ values in the expressions described in detail elsewhere [10, 47].

Results and discussion

XRD patterns and degree of crystallinity

Figure 1 presents the XRD patterns of PEO-*x* wt% SnO₂ films in the 2θ range from 10° to 55°. Figure 1a shows that the pristine PEO film has characteristic intense peaks at 19.22° (120) and 23.41° (112),(032) of its major crystalline phases [35–37]. Some peaks of relatively low intensities at 14.71°, 15.18°, 22.11°, 26.26°, 27.0°, and 27.93° are also observed in the XRD pattern of PEO film. It can be noted from the figure that the dispersion of 1, 3, and 5 wt% SnO₂ amounts into the PEO matrix enormously alters the intensities of the main peaks of PEO. The initial loading of 1 wt% amount of SnO₂ highly increased the intensity of 19.22° peak and largely reduced the 23.41° peak in comparison with the intensities of pristine PEO film. Here, in the XRD patterns, the peaks intensities denote the content of respective crystalline phases. The XRD results confirm that the interactions between the SnO₂ nanoparticles and the PEO chain structures in the PNC film have resulted in a massive redistribution of phase concentration of the different PEO crystallites. Furthermore, the relative variation in the intensities of PEO peaks with further increase in SnO₂ concentration up to 5 wt% infers that the polymer–nanoparticle interactions vary significantly with the filler concentration in these PNC films. In comparison with the intensity of major PEO peak exhibited at 19.22°, the SnO₂ nanofiller peaks intensities in these PNC films are found very low which can be seen in the coloured highlighted part in Fig. 1a.

Figure 1b shows the enlarged view of XRD patterns of the PNC films over the angular range 25°–55° in which the characteristic diffraction peaks of SnO₂ crystallites can be clearly noted as these are highlighted by a coloured background. The SnO₂ nanopowder of tetragonal rutile phase used in the preparation of these PNC films exhibits major diffraction peaks at 26.58° (110), 33.87° (101), 37.96° (200), and 51.79° (211) (see upper layer of Fig. 1b) which corroborates with earlier results [19, 26]. From Fig. 1b, one can read from the marked scale that the intensities of SnO₂ peaks gradually enhance with the increase in its concentration in the PEO

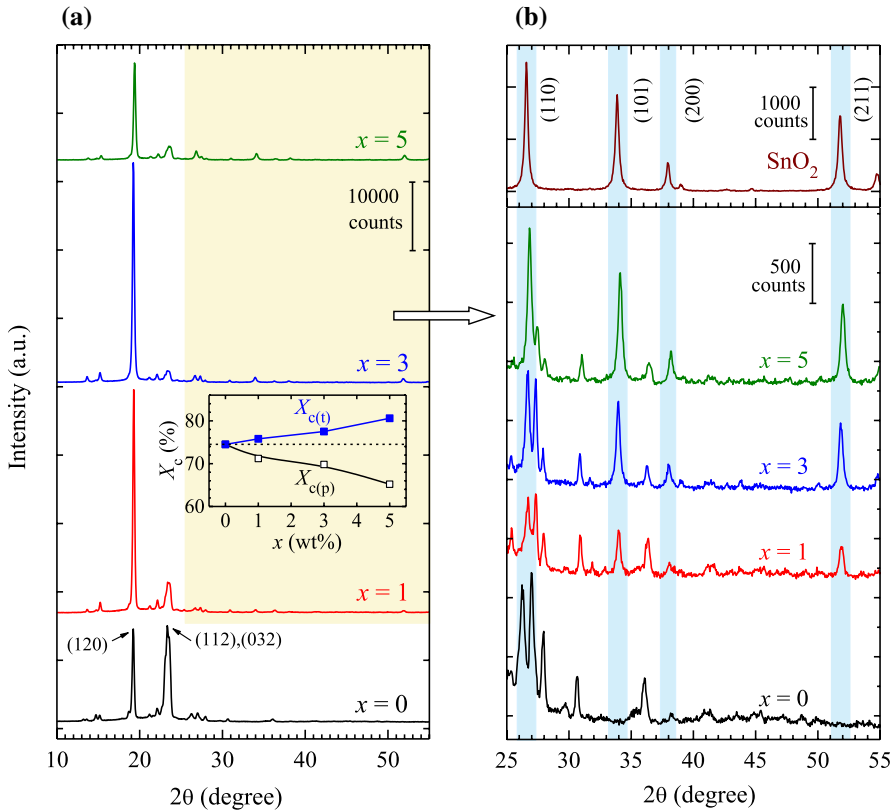


Fig. 1 **a** XRD patterns of PEO-*x* wt% SnO₂ films for *x*=0, 1, 3, and 5 and **b** enlarged view of the XRD patterns over the angular range from 25° to 55° showing the SnO₂ diffraction peaks (highlighted) in the PNC films for their comparison with the peaks of SnO₂ nanopowder (upper layer). The inset of **a** shows the plot of $X_{c(p)}$ and $X_{c(t)}$ versus *x* (wt%) concentration of SnO₂ in the PNC films

matrix which is an evidence of the homogeneously dispersed SnO₂ nanoparticles in the polymer structures and this result firmly confirms the formation of good quality nanocomposites. Further, the angular positions of SnO₂ peaks are unaltered with the increase in its concentration in the PNC films, revealing that the SnO₂ nanoparticles retain their crystallite structure in the films.

The degree of crystallinity of the PEO matrix $X_{c(p)}$ in PNC films and that of the total PNC material $X_{c(t)}$ were determined using the relations $X_{c(p)} (\%) = (A_{c(p)} / (A_{c(p)} + A_a)) \times 100$ and $X_{c(t)} (\%) = (A_{c(t)} / (A_{c(t)} + A_a)) \times 100$, respectively, which are demonstrated earlier [38–40]. In these relations, the areas of crystalline peaks ($A_{c(p)}$) for the PEO peaks and total area of crystalline peaks $A_{c(t)}$ including both PEO and SnO₂ peaks) and that of the amorphous hump (A_a) were computed from the XRD pattern of each film using the OriginPro® software. The determined values of $X_{c(p)}$ and $X_{c(t)}$ of these materials are plotted in the inset in Fig. 1a. It can be noted from this plot that the increase in SnO₂ concentration reduces the crystallinity of the PEO

matrix, whereas the total crystalline content of PNC material increases a little due to the SnO_2 crystallites in these materials.

SEM images and morphological analysis

The SEM images of the surface and fractured cross section of PEO-1 wt% SnO_2 and PEO-5 wt% SnO_2 films are shown in Fig. 2. These images reveal the homogeneous distribution of the SnO_2 nanoparticles in the polymer matrix, and there is no noticeable signature of agglomerated nanoparticles which confirms the formation of good quality nanocomposites. Further, some typical spherulite structures of PEO crystallites [39, 48] are encircled in the SEM image of 1 wt% SnO_2 -containing PNC material (Fig. 2a), and the presence of nanoparticles is highlighted by small circles for the 5 wt% SnO_2 -containing PNC film (Fig. 2c).

FTIR spectra and polymer–nanofiller interaction

Figure 3 presents the FTIR spectra of PEO- x wt% SnO_2 films over the wavenumber range from 650 to 1600 cm^{-1} . The wavenumbers of various vibrations bands of the pristine PEO film are marked by dashed vertical lines in the figure which are attributed to its characteristic vibrational modes demonstrated in detail in the literature [9, 39, 48]. A close look on the figure reveals that the FTIR spectrum of each PNC film

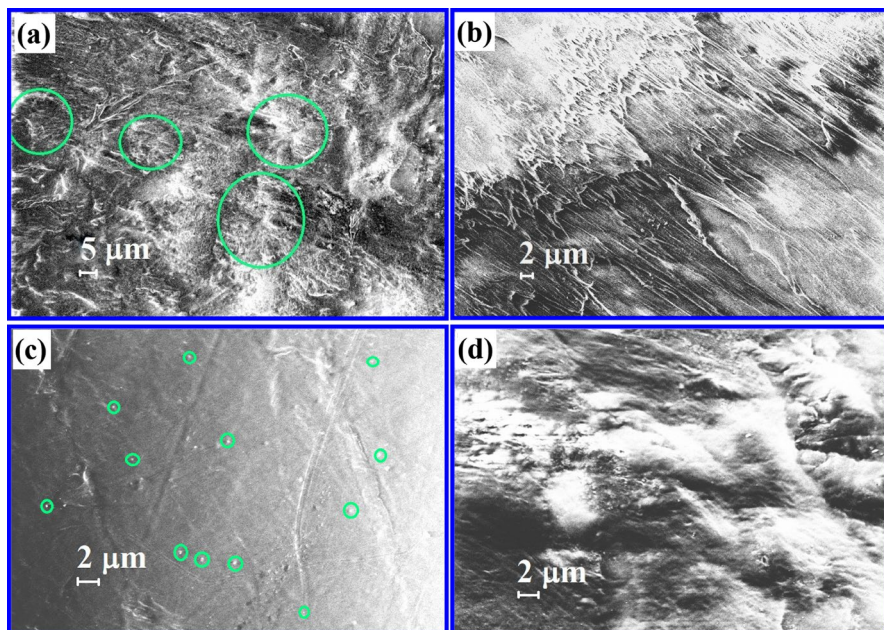


Fig. 2 SEM images of PEO- x wt% SnO_2 films for $x=1$ (**a** surface and **b** fractured) and for $x=5$ (**c** surface and **d** fractured). PEO spherulites are encircled in **a** and SnO_2 nanoparticles are encircled in **c**

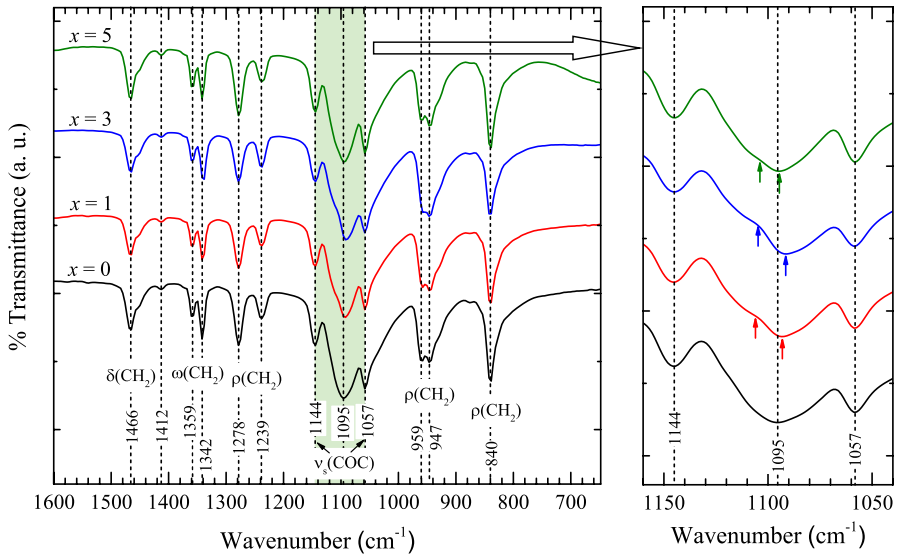


Fig. 3 FTIR spectra of PEO-*x* wt% SnO₂ films for *x*=0, 1, 3, and 5. Wavenumbers of various vibrational bands of the pristine PEO film are marked in the figure. The enlarged view of –C–O–C– vibrational bands is shown on the right side of the main figure

fairly resembles that of the pristine PEO film except a little change in the intensities of some of the peaks. However, it can be noted from the enlarged view presented on the right side of the main plot that the symmetric and asymmetric stretching modes of –C–O–C– group have little changes in the peaks positions marked by arrows and some broadening of the bands with the increase in SnO₂ concentration in the PNC films as compared to the pristine PEO film [7, 48]. These results confirm that there are no strong chemical interactions between the PEO functional group and SnO₂ nanoparticles in the nanocomposite films because chemical interactions largely modify the shape of the bands and their peaks positions [47]. In such a case, the presence of SnO₂ nanoparticles would predominantly act as physical confinement for PEO chains which can lead to alteration in their molecular packing and crystallites as revealed from the XRD results of these materials. Similar behaviour of polymer–nanoparticle interactions was also reported for the silica nanoparticles dispersed PEO matrix-based PNC films [49].

Dielectric spectra and polarization processes

Figure 4 shows the complex dielectric permittivity (real part ϵ' and imaginary part ϵ'') and dielectric loss tangent ($\tan\delta = \epsilon''/\epsilon'$) spectra of PEO-*x* wt% SnO₂ films at 30 °C (Fig. 4a) and also at different temperatures for the PEO-3 wt% SnO₂ film (Fig. 4b). The ϵ' values of these materials nonlinearly decrease with the increase in frequency from 20 Hz to about 300 kHz, and after that, they slowly approach a steady-state value near 1 MHz. A sharp decrease in ϵ' values has been noted with

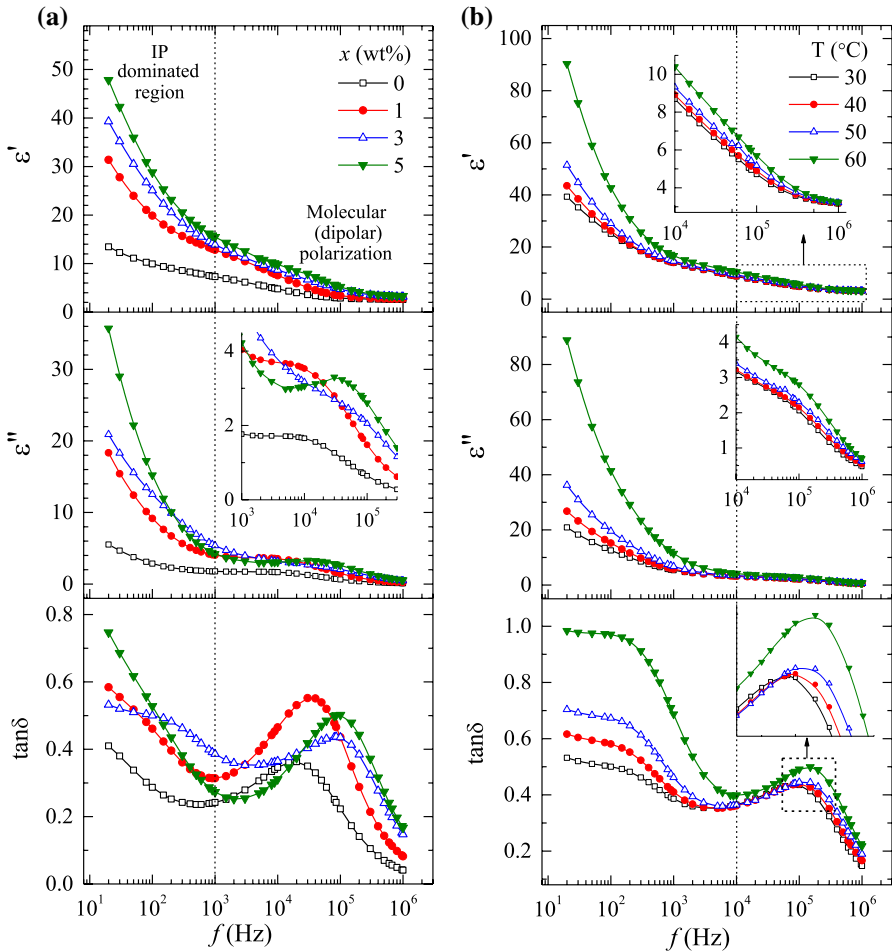


Fig. 4 Spectra of complex permittivity (real part ϵ' and loss part ϵ'') and dielectric loss tangent $\tan\delta$ of **a** PEO- x wt% SnO₂ films for $x=0, 1, 3,$ and $5,$ at $30\text{ }^\circ\text{C},$ and **b** PEO- 3 wt% SnO₂ film at temperatures in the range $30\text{--}60\text{ }^\circ\text{C}.$ Insets show the enlarged view of the spectra at higher frequencies

the increase in frequency in the lower-frequency region (i.e. 20 Hz–1 kHz). Further, it is found that the ϵ' value increased by more than two times at 20 Hz with the dispersion of 1 wt% amount of SnO₂ in the PEO matrix in comparison with that of the pristine PEO film, and it increased by about four times with the further increase in SnO₂ concentration up to 5 wt% in the PEO matrix. Figure 4a shows that the relative increase in ϵ' values of PNC films diminishes as the frequency of alternating field increases. The huge increase in ϵ' values in the low-frequency region is obviously caused by interfacial polarization (IP) effect which is also known as Maxwell–Wagner–Sillars (MWS) polarization mechanism and is a common phenomenological characteristic of the PNC materials [6, 9, 10, 12, 19, 31, 35–40, 50, 51]. However, at higher frequencies, the IP effect cannot synchronize with fast reversible changes

in the ac field [12, 29], and therefore, its contribution to the dielectric polarization is insignificant, and hence, the observed ϵ' values are primarily attributed to the dipolar reorientation and the electronic polarization processes of these films [9, 10]. Similar to these results on the dielectric dispersion of PEO/SnO₂ films, the increased ϵ' values have also been reported for the PNC films of SnO₂ dispersed PVDF matrix [52] and also the PEO/PVP blend matrix-based nanocomposite films [49].

Further, it is found that the dielectric dispersion behaviour and the contribution of IP effect in the ϵ' values of PEO-*x* wt% SnO₂ films are extremely different in comparison with those of the PEO-*x* wt% SiO₂ [35], PEO-*x* wt% Al₂O₃ [36], and PEO-*x* wt% ZnO [37] nanocomposite films. This difference in dielectric dispersion may be owing to the relatively very high dielectric constant of SnO₂ as compared to that of the SiO₂, Al₂O₃ and ZnO materials [26]. Furthermore, the effect of the differences in these nanofiller particles shapes and sizes [26, 27] on the observed dielectric properties cannot be ruled out because the dielectric constant of the PNC materials is significantly influenced by the particles size of the nanofillers [22]. The ϵ'' spectra of these PNC films reveal that there is a huge contribution of the IP effect in the dielectric loss at low frequencies due to which the ϵ'' decreases sharply with the increase in frequency up to 1 kHz. Further, a low-intensity relaxation peak or hump is exhibited in the intermediate-frequency region which can be noted in the enlarged view of the ϵ'' spectra given in inset of the figure, and the same can be assigned to the PEO chain segmental motion relaxation process [35–37, 53].

Figure 4b shows the ϵ' and ϵ'' spectra of PEO-3 wt% SnO₂ film at different temperatures which is studied as a representative sample of these PNC films. It can be noted from the figure that the effect of temperature on the increase in ϵ' and ϵ'' values is relatively small in the high-frequency region, whereas below 1 kHz these values at fixed frequency sharply enhance with the increase in temperature. This finding confirms the thermally activated dielectric polarization behaviour of this PNC film which is frequently observed in the PNC materials [10, 12, 16, 30, 36, 40, 51]. Further, the increase in ϵ' values in the low-frequency region at 60 °C is relatively very high which may be owing to the fact that this temperature value is closer to the melting temperature of PEO (i.e. ~65 °C). This temperature has resulted in higher free volume which further facilitates the dipole orientation and their parallel ordering in the PEO chains. From these results, it is also unveiled that the IP effect dominating at lower frequencies is more sensitive to the temperature of the PNC film, while the temperature is comparatively less effective on the molecular polarization of the film at higher frequencies. Furthermore, 50 Hz, 1 kHz, and 1 MHz frequencies values of ϵ' and ϵ'' for the PEO-*x* wt% SnO₂ films at 30 °C and also those of the PEO-3 wt% SnO₂ film at different temperatures are recorded in Table 1 for the relative comparison and examining the changes with nanofiller content as well as temperature variation.

The $\tan\delta$ spectra of PEO-*x* wt% SnO₂ films exhibit the dielectric relaxation peaks above 10 kHz at 30 °C (Fig. 4a), which may be assigned to the local chain segmental motion of PEO (α -relaxation in the amorphous part [53]). This relaxation was also observed in the PEO matrix-based different nanofillers dispersed PNC films studied earlier [35–37]. It can be noted from the $\tan\delta$ plots that the relaxation peaks of these PNC films are relatively more intense and have appeared

Table 1 Values of complex dielectric permittivity $\epsilon' - j\epsilon''$ (at 50 Hz, 1 kHz, and 1 MHz), dielectric relaxation time τ_s , electric modulus relaxation time τ_M , and dc electrical conductivity (determined from low-frequency σ' spectra $\sigma_{dc(e)}$ and the high-frequency spectra $\sigma_{dc(i)}$) of the PEO- x wt% SnO₂ films at 30 °C, and also for the PEO-3 wt% SnO₂ film at different temperatures T

PNC films	$\epsilon' - j\epsilon''$			τ_s (μ s)	τ_M (μ s)	$\sigma_{dc(e)}$ ($\times 10^{-11}$ S/ cm)	$\sigma_{dc(i)}$ ($\times 10^{-7}$ S/ cm)
	50 Hz	1 kHz	1 MHz				
PEO- x wt% SnO ₂ films							
x (wt%)							
0	11.1- j 3.75	7.3- j 1.77	2.6- j 0.11	8.89	3.86	0.97	0.32
1	24.0- j 12.41	12.4- j 4.03	2.8- j 0.23	4.55	1.85	1.69	0.76
3	30.5- j 15.57	13.9- j 5.36	3.2- j 0.47	1.85	0.83	3.05	1.47
5	36.0- j 22.19	15.5- j 4.22	3.3- j 0.55	1.78	0.77	10.8	1.63
PEO-3 wt% SnO ₂ film							
T (°C)							
30	30.5- j 15.57	13.9- j 5.36	3.2- j 0.47	1.85	0.83	3.05	1.47
40	32.7- j 19.42	14.1- j 5.77	3.2- j 0.53	1.73	0.72	4.41	1.80
50	37.3- j 25.47	14.6- j 6.73	3.2- j 0.61	1.36	0.56	6.49	2.16
60	59.0- j 57.48	16.6- j 11.43	3.2- j 0.71	1.12	0.47	21.1	2.68

at higher frequencies as compared to that of the pristine PEO film which confirms that the number of relaxing dipoles in the polymer chain have enhanced in the presence of SnO₂ nanoparticles which also promote the chain segmental motion. The values of dielectric relaxation time τ_s (τ_α) for these materials were determined from the $\tan\delta$ peak frequency f_p values from the relation $\tau_s = (2\pi f_p)^{-1}$. The obtained τ_s values for these PNC materials are listed in Table 1. It is noted that the τ_s values of these PNC films are lower than that of the pristine PEO film which confirms that the SnO₂ nanoparticles accelerate the chain segmental motion of PEO which is owing to the fact that the crystalline phase content of the polymer has decreased (see inset in Fig. 1a). The increase in chain segmental dynamics as well as the increase in the amount of amorphous phase favours the suitability of these PNC materials as host matrices for the preparation of promising properties solid polymer electrolytes (SPEs) [28, 45].

From the enlarged view of Fig. 4b, it can be noted that the relaxation peak of $\tan\delta$ spectra gradually shifts towards high-frequency side along with a small increase in its magnitude when the temperature of PEO-3 wt% SnO₂ film enhances from 30 to 60 °C. This result also evidences the increase in the number of relaxing dipoles with the faster chain segmental motion which happens due to the increase in the free volume in the material. The temperature-dependent τ_s values of this PNC film were also determined using f_p values from the $\tan\delta$ spectra and these are recorded in Table 1. Further, from the relative changes in the shape of these $\tan\delta$ spectra in the low-frequency region, it seems that there is signature of low-frequency relaxation process in these materials corresponding to the MWS mechanism, but it is not clearly distinguishable in these spectra; however, the same is clearly noticed in the electric modulus spectra given in the following section.

Electric modulus spectra and relaxation processes

The complex electric modulus (real part M' and imaginary part M'') spectra of PEO- x wt% SnO₂ films at 30 °C and also that of the PEO-3 wt% SnO₂ film with the temperature variation are presented in Fig. 5. Because of the inverse relation between the dielectric and electric modulus functions, the M' and M'' spectra remain free from electrode polarization (EP) effect, adsorbed impurities, and the electrode material of the dielectric test fixture, and therefore, these spectra are frequently analysed for better resolution of the relaxation processes in the composite materials [7, 9, 10, 12, 17, 18, 30, 39, 51]. Figure 5a shows that there is a gradual increase in M' values with the increase in frequency in the lower-frequency region, and then, there is an abrupt rise in the high-frequency region and they finally attain a steady-state near 1 MHz. This dispersion behaviour of M' spectra is also observed for several other PNC materials [9–12, 35–38]. The M'' spectra of these materials exhibit broader and low-intensity MWS relaxation peaks in the lower-frequency region, whereas sharp and intense conductivity relaxation peaks associated with the chain segmental motion in amorphous domains of PEO have appeared in the high-frequency region.

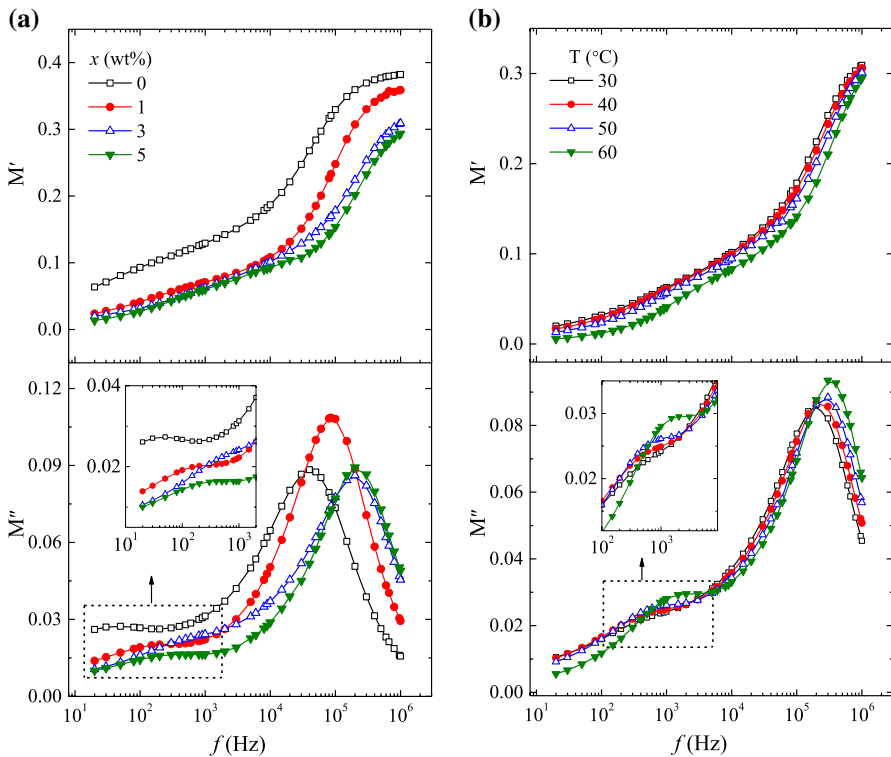


Fig. 5 Spectra of electric modulus (real part M' and loss part M'') of **a** PEO- x wt% SnO₂ films for $x=0, 1, 3,$ and $5,$ at $30\text{ }^{\circ}\text{C},$ and **b** PEO-3 wt% SnO₂ film at temperatures in the range $30\text{--}60\text{ }^{\circ}\text{C}.$ Insets show the enlarged view of the low-frequency relaxation peaks

The frequency and intensity of the relaxation peak vary with the increase in SnO₂ content in these PNC films which confirm that these relaxation processes are significantly affected by the amount of nanofiller in the PEO matrix. Further, a little shift of intense loss peak to higher frequencies with the increase in nanofiller content is an indication of low interactions between SnO₂ nanoparticles and the PEO chains, and also weak adhesion in these composites which further favours the FTIR results of these materials. These relaxation processes are also found temperature dependent as can be seen from the M'' spectra of PEO-3 wt% SnO₂ film presented in Fig. 5b. The modulus relaxation time τ_M also known as conductivity relaxation of these materials was determined using the intense peak frequency values and observed τ_M values are reported in Table 1. One can read from this table that the values of τ_M are about half order of magnitude low as compared to the τ_s values for these PEO- x wt% SnO₂ materials. This is a common trend of variation in the relaxation times of PNC materials when they are analysed using dielectric and electric modulus functions [10, 34–36, 40].

AC and DC electrical conductivities

The alternating current (ac) electrical conductivity (real part σ') spectra of PEO- x wt% SnO₂ films at 30 °C and those of the PEO-3 wt% SnO₂ film with the temperature variation are depicted in Fig. 6. Figure 6a shows that the σ' value of PEO film is of the order of 10⁻¹¹ S/cm at 20 Hz and there is an increase of about one order of magnitude at the same frequency when 5 wt% amount of SnO₂ was dispersed in the PEO matrix. The σ' values of PEO-3 wt% SnO₂ film also enhance by about one order of magnitude with the increase in film temperature from 30 to 60 °C (Fig. 6b). Further, the σ' values exhibit a relatively fast increase with the increase in frequency up to about 100 kHz, and thereafter, the rate of increase is small. This type of conductivity dispersion behaviour of the PEO matrix-based PNC films is due

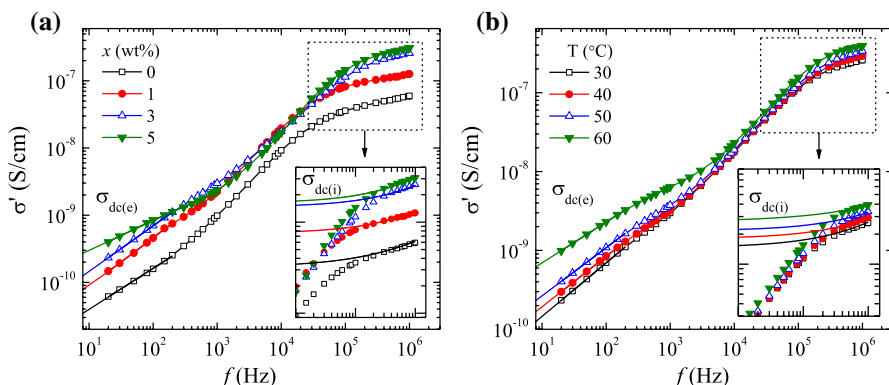


Fig. 6 Spectra of ac electrical conductivity (real part σ') of **a** PEO- x wt% SnO₂ films for $x=0, 1, 3,$ and $5,$ at 30 °C and **b** PEO-3 wt% SnO₂ film at different temperatures. Insets show the power law fit of σ' values of high-frequency region. The solid lines show the linear behaviour of σ' values in the low-frequency region

to semicrystalline nature of the host matrix as demonstrated earlier [35–47]. The enhancement of σ' values of these materials reveals that there may be an increase in number of free charges and/or formation of some favourable charge conductive paths due to the polymer–nanoparticle electrostatic interactions.

The direct current (dc) electrical conductivity σ_{dc} of these materials was estimated by linear fit of low-frequency σ' data for electronic conduction (denoted by $\sigma_{dc(e)}$) and the power law fit $\sigma' = \sigma_{dc} + A\omega^n$ of high-frequency σ' data for probable ionic conduction (denoted by $\sigma_{dc(i)}$). These fits are shown by solid lines in Fig. 6. The observed values of $\sigma_{dc(e)}$ and $\sigma_{dc(i)}$ for the PEO- x wt% SnO₂ films at 30 °C and also for the PEO-3 wt% SnO₂ film with its temperature variation are recorded in Table 1. It can be read from this table that the σ_{dc} values increase with the increase in SnO₂ concentration in the PNC films and also with the increase in temperature of the PNC film.

Relaxation times and conductivity plots

Figure 7a shows the variation of τ_s , τ_M , $\sigma_{dc(e)}$, and $\sigma_{dc(i)}$ against x (wt%) amount of SnO₂ in the PNC films at 30 °C. It can be noted from this figure that both the relaxation times nonlinearly decrease with the increase in SnO₂ concentration up to 5 wt% in the PNC films, whereas their conductivities nonlinearly increase. This finding confirms that the charge conduction mechanism is associated with the structural relaxation processes of the polymer matrix which is one of the important facts in regard to the suitability of these materials as host matrix for the preparation of novel SPEs.

The logarithmic scale τ_s , τ_M , $\sigma_{dc(e)}$, and $\sigma_{dc(i)}$ versus $1000/T$ plots of the PEO-3 wt% SnO₂ film are shown in Fig. 7b. The straight line behaviour of these

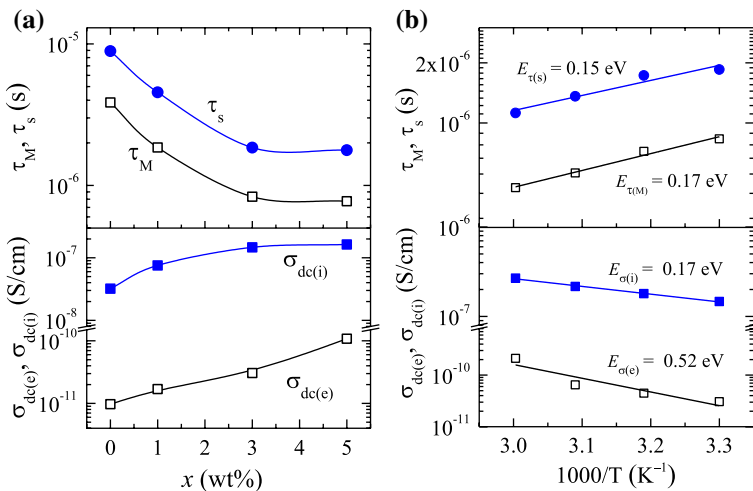


Fig. 7 Plots of **a** τ_M , τ_s , $\sigma_{dc(e)}$, and $\sigma_{dc(i)}$ versus x (wt%) for PEO- x wt% SnO₂ films, and **b** τ_M , τ_s , $\sigma_{dc(e)}$, and $\sigma_{dc(i)}$ versus $1000/T$ for the PEO-3 wt% SnO₂ film

plots confirms that the relaxation times and electrical conductivities obey the Arrhenius relations $\tau = \tau_0 \exp(E_\tau/k_B T)$ (where E_τ is the activation energy of relaxation time) and $\sigma_{dc} = \sigma_0 \exp(-E_\sigma/k_B T)$ (where E_σ is the conductivity activation energy), respectively. The evaluated values of E_τ and E_σ are given with the respective plots in this figure. The E_τ and E_σ values of the PNC film are found significantly small (0.15–0.17 eV) except $E_{\sigma(e)}$ which suggest that there is a low potential barrier for the ionic charge transportation and the relaxation mechanism. This fact also confirms the suitability of the PNC material as a nanocomposite base matrix for the preparation of high-performance solid polymer electrolytes with the doping of alkali metal ionic salts in appropriate amount.

Conclusions

The crystallographic study of PEO-*x* wt% SnO₂ films reveals a huge alteration in crystals phase concentration of the PEO due to polymer–nanoparticle electrostatic interactions. A uniform increase in the intensities of SnO₂ characteristic diffraction peaks with the increase in its amount in the PEO matrix confirms the homogeneity of the nanoparticles in the nanocomposites which is also concluded by their SEM images. The percentage degree of crystallinity of the host PEO matrix nonlinearly decreases with the increase in SnO₂ concentration, but there is a uniform increase in crystallinity of the bulk composite material. The FTIR results evidence weak chemical but appreciable electrostatic interactions of the SnO₂ nanoparticles with the dipolar groups of PEO chains. The dielectric and electrical properties of PEO-*x* wt% SnO₂ films for *x* values 0, 1, 3, and 5 are reported over the frequency range 20 Hz–1 MHz, at 30 °C, and also with temperature variation for the PEO-3 wt% SnO₂ film as a representative sample. The spectra of complex dielectric permittivity, electric modulus, and ac electrical conductivity for these materials were analysed, and the effect of SnO₂ concentration and the temperature on these electrical functions was explored. The dispersion of SnO₂ nanoparticles produces high interfacial polarization at low frequencies and also favours the dipole ordering at high frequencies due to which the complex permittivity of these PNC materials significantly increases. A weak relaxation peak was observed in the low-frequency region of the electric modulus spectra which is corresponding to the MWS relaxation process, whereas a highly intense relaxation peak appeared in the high-frequency region attributing to the conductivity relaxation associated with the PEO chain segmental motion. The presence of SnO₂ nanoparticles in the PEO structures increases the chain segmental dynamics and also the electrical conductivity of these nanocomposites. The dielectric permittivity and electrical conductivity significantly enhance with the increase in temperature of the PNC film confirming its thermally activated dielectric behaviour. The relaxation time and dc electrical conductivity of the PNC film obey Arrhenius relation with appreciably low activation energies. The enhancement of dielectric permittivity with the nanofiller concentration suggests the suitability of these materials as tunable nanodielectrics which could be promising dielectric substrates and insulators in the fabrication of flexible-type advanced

microelectronic devices including the high-density energy storing capacitors. The increased chain segmental dynamics, lowering in degrees of crystallinity of polymer matrix, and also the low activation energies altogether make these nanomaterials more advantageous in the preparation of nanocomposite solid polymer electrolytes.

Acknowledgements The author (PD) appreciatively acknowledges the Council of Scientific and Industrial Research (CSIR), New Delhi, for the award of Postdoctoral Fellowship (Research Associate).

References

1. Guo JZ, Song K, Liu C (2019) Polymer-based multifunctional nanocomposites and their applications. Elsevier Inc, Amsterdam
2. Tan D, Irwin P (2011) Polymer based nanodielectric composites. In: Sikalidis C (ed) Advances in ceramics. INTECH, Croatia
3. Tanaka T, Vaughan AS (2017) Tailoring of nanocomposite dielectrics: from fundamentals to devices and applications. Temasek Boulevard, Pan Stanford Publishing Pte Ltd., Singapore
4. Dang ZM, Yuan JK, Yao SH, Liao RJ (2013) Flexible nanodielectric materials with high permittivity for power energy storage. *Adv Mater* 25:6334–6365
5. Luzio A, Ferré FG, Fonzo FD, Caironi M (2014) Hybrid nanodielectrics for low-voltage organic electronics. *Adv Funct Mater* 24:1790–1798
6. Alghunaim NS, Alhusaiki-Alghamdi HM (2019) Role of ZnO nanoparticles on the structural, optical and dielectric properties of PVP/PC blend. *Phys B Condens Matter* 560:185–190
7. Morsi MA, Rajeh A, Al-Muntaser AA (2019) Reinforcement of the optical, thermal and electrical properties of PEO based on MWCNTs/Au hybrid fillers: nanodielectric materials for organo-electronic devices. *Compos Part B* 173:106957
8. Anandraj J, Joshi GM (2018) Fabrication, performance and applications of integrated nanodielectric properties of materials—a review. *Compos Interfaces* 25:455–489
9. Sengwa RJ, Choudhary S, Dhatarwal P (2019) Nonlinear optical and dielectric properties of TiO₂ nanoparticles incorporated PEO/PVP blend matrix based multifunctional polymer nanocomposites. *J Mater Sci: Mater Electron* 30:12275–12294
10. Choudhary S, Sengwa RJ (2018) ZnO nanoparticles dispersed PVA–PVP blend matrix based high performance flexible nanodielectrics for multifunctional microelectronic devices. *Curr Appl Phys* 18:1041–1058
11. Singh R, Bajpai AK, Shrivastava AK (2020) CdSe nanorod-reinforced poly(thiophene) composites in designing energy storage devices: Study of morphology and dielectric behavior. *Polym Bull.* <https://doi.org/10.1007/s00289-020-03104-8>
12. Tsonos C, Zois H, Kanapitsas A, Soin N, Siores E, Peppas GD, Pyrgioti EC, Sanida A, Stavropoulos SG, Psarras GC (2019) Polyvinylidene fluoride/magnetite nanocomposites: dielectric and thermal response. *J Phys Chem Solids* 129:378–386
13. Nguyen TP (2011) Polymer-based nanocomposites for organic optoelectronic devices A review. *Surf Coat Technol* 206:742–752
14. Piana F, Kredatusová J, Paruzel B, Pflieger J (2017) Polymer blends of poly(2-cyanoethyl vinyl ether) and poly(methyl methacrylate) with improved dielectric properties for flexible electronics. *Express Polym Lett* 11:731–737
15. Kandulna R, Choudhary RB (2018) Concentration-dependent behaviors of ZnO-reinforced PVA–ZnO nanocomposites as electron transport materials for OLED application. *Polym Bull* 75:3089–3107
16. Bouropoulos N, Psarras GC, Moustakas N, Chrissanthopoulos A, Baskoutas S (2008) Optical and dielectric properties of ZnO-PVA nanocomposites. *Phys Stat Sol A* 205:2033–2037
17. Patsidis A, Psarras GC (2008) Dielectric behaviour and functionality of polymer matrix—ceramic BaTiO₃ composites. *Express Polym Lett* 2:718–726

18. Abouhaswa AS, Taha TA (2019) Tailoring the optical and dielectric properties of PVC/CuO nanocomposites. *Polym Bull.* <https://doi.org/10.1007/s00289-019-03059-5>
19. Sarkar PK, Bhattacharjee S, Prajapat M, Roy S (2015) Incorporation of SnO₂ nanoparticles in PMMA for performance enhancement of a transparent organic resistive memory device. *RSC Adv* 5:105661–105667
20. Tsonos C, Soin N, Tomara G, Yang B, Psarras GC, Kanapitsasa A, Siores E (2016) Electromagnetic wave absorption properties of ternary poly(vinylidene fluoride)/magnetite nanocomposites with carbon nanotubes and graphene. *RSC Adv* 6:1919–1924
21. Xu F, Zhang H, Jin L, Li Y, Li J, Gan G, Wei M, Li M, Liao Y (2018) Controllably degradable transient electronic antennas based on water-soluble PVA/TiO₂ films. *J Mater Sci* 53:2638–2647
22. Bi M, Hao Y, Zhang J, Lei M, Bi K (2017) Particle size effect of BaTiO₃ nanofillers on the energy storage performance of polymer nanocomposites. *Nanoscale* 9:16386–16395
23. Kar E, Bose N, Dutta B, Banerjee S, Mukherjee N, Mukherjee S (2019) 2D SnO₂ nanosheet/PVDF composite based flexible, self-cleaning piezoelectric energy harvester. *Energy Convers Manag* 184:600–608
24. Krehula LK, Stjepanović J, Perlog M, Krehula S, Gilja V, Travas-Sejdic J, Hrnjak-Murčić Z (2019) Conducting polymer polypyrrole and titanium dioxide nanocomposites for photocatalysis of RR₄₅ dye under visible light. *Polym Bull* 76:1697–1715
25. Bahuleyan BK, Induja C, Ramesan MT (2019) Influence of titanium dioxide nanoparticles on the structural, thermal, electrical properties, and gas sensing behavior of polyaniline/phenothiazine blend nanocomposites. *Polym Compos* 40:4416–4426
26. Choudhary S, Sengwa RJ (2017) Effects of different inorganic nanoparticles on the structural, dielectric and ion transportation properties of polymers blend based nanocomposite solid polymer electrolytes. *Electrochim Acta* 247:924–941
27. Dhatarwal P, Choudhary S, Sengwa RJ (2018) Electrochemical performance of Li⁺-ion conducting solid polymer electrolytes based on PEO–PMMA blend matrix incorporated with various inorganic nanoparticles for the lithium ion batteries. *Compos Commun* 10:11–17
28. Channu VSR, Rambabu B, Kumari K, Kalluru RR, Holze R (2018) SnO₂/PANI nanocomposite electrodes for supercapacitors and lithium ion batteries. *Electrochim Energy Technol* 4:32–38
29. Mao F, Shi Z, Wang J, Zhang C, Yang C, Huang M (2018) Improved dielectric permittivity and retained low loss in layer-structured films via controlling interfaces. *Adv Compos Hybrid Mater* 1:548–557
30. Mathioudakis GN, Patsidis AC, Psarras GC (2014) Dynamic electrical thermal analysis on zinc oxide/epoxy resin nanodielectrics. *J Therm Anal Calorim* 116:27–33
31. Smith RC, Liang C, Landry M, Nelson JK, Schadler LS (2008) The mechanisms leading to the useful electrical properties of polymer nanodielectrics. *IEEE Trans Dielectr Electr Insul* 15:187–196
32. Singh PK, Goyal P, Sharma A, Rajesh KD, Gaur MS (2018) Effect of interface in dielectric relaxation properties of PEMA–BaZrO₃ nanocomposites. *Polym Bull* 75:4003–4018
33. Alhabill FN, Ayoob R, Andritsch T, Vaughan AS (2018) Introducing particle interphase model for describing the electrical behaviour of nanodielectrics. *Mater Design* 158:62–73
34. Sengwa RJ, Choudhary S, Sankhla S (2010) Dielectric properties of montmorillonite clay filled poly(vinyl alcohol)/poly(ethylene oxide) blend nanocomposites. *Compos Sci Tech* 70:1621–1627
35. Choudhary S, Sengwa RJ (2015) Dielectric dispersion and relaxation studies of melt compounded poly(ethylene oxide)/silicon dioxide nanocomposites. *Polym Bull* 72:2591–2604
36. Sengwa RJ, Choudhary S (2017) Dielectric and electrical properties of PEO–Al₂O₃ nanocomposites. *J Alloys Compd* 701:652–659
37. Choudhary S, Sengwa RJ (2017) Morphological, structural, dielectric and electrical properties of PEO–ZnO nanodielectric films. *J Polym Res* 24:54
38. Sengwa RJ, Choudhary S, Dhatarwal P (2019) Investigation of alumina nanofiller impact on the structural and dielectric properties of PEO/PMMA blend matrix-based polymer nanocomposites. *Adv Compos Hybrid Mater* 2:162–175
39. Dhatarwal P, Sengwa RJ (2019) Impact of PVDF/PEO blend composition on the β-phase crystallization and dielectric properties of silica nanoparticles incorporated polymer nanocomposites. *J Polym Res* 26:196
40. Choudhary S, Sengwa RJ (2019) Investigation on structural and dielectric properties of silica nanoparticles incorporated poly(ethylene oxide)/poly(vinyl pyrrolidone) blend matrix based nanocomposites. *J Inorg Organomet Polym* 29:592–607

41. Choudhary S (2017) Structural and dielectric properties of (PEO–PMMA)–SnO₂ nanocomposites. *Compos Commun* 5:54–63
42. Orlandi MO (2020) Tin oxide materials: synthesis, properties, and applications. Elsevier Inc., Amsterdam
43. Jian KS, Chang CJ, Wu JJ, Chang YC, Tsay CY, Chen JH, Horng TL, Lee GJ, Karuppasamy L, Anandan S, Chen CY (2019) High response CO sensor based on a polyaniline/SnO₂ nanocomposite. *Polymers* 11:184
44. Dhinakar KG, Selvalakshmi T, Sundar SM, Bose AC (2016) Structural, optical and impedance properties of SnO₂ nanoparticles. *J Mater Sci Mater Electron* 27:5818–5824
45. Xiong HM, Zhao KK, Zhao X, Wang YW, Chen JS (2003) Elucidating the conductivity enhancement effect of nano-sized SnO₂ fillers in the hybrid polymer electrolyte PEO–SnO₂–LiClO₄. *Solid State Ionics* 159:89–95
46. Thakur AK, Hashmi SA (2010) Polymer matrix-filler interaction mechanism for modified ion transport and glass transition temperature in the polymer electrolyte composites. *Solid State Ionics* 181:1270–1278
47. Sengwa RJ, Dhatarwal P (2020) Predominantly chain segmental relaxation dependent ionic conductivity of multiphase semicrystalline PVDF/PEO/LiClO₄ solid polymer electrolytes. *Electrochim Acta* 338:135890
48. Dhatarwal P, Sengwa RJ (2019) Polymer compositional ratio-dependent morphology, crystallinity, dielectric dispersion, structural dynamics, and electrical conductivity of PVDF/PEO blend films. *Macromol Res* 27:1009–1023
49. Utpalla P, Sharma SK, Sudarshan K, Kumar V, Pujari PK (2019) Free volume correlation with ac conductivity and thermo-mechanical properties of poly(ethylene oxide)-silica nanocomposites. *Eur Polym J* 117:10–18
50. Morsi MA, Abdelaziz M, Oraby A, Makhles I (2019) Structural, optical, thermal, and dielectric properties of polyethylene oxide/carboxymethyl cellulose blend filled with barium titanate. *J Phys Chem Solids* 125:103–114
51. Alhusaiki-Alghamdi HM (2019) Improve spectroscopic structural and AC electrical conductivity of PC/PEO blend using grapheme. *Res Phys* 12:793–798
52. Liu Z, Wang F, Zhu H (2016) Enhanced dielectric properties of polyvinylidene fluoride with addition of SnO₂ nanoparticles. *Phys Status Solidi RRL* 10:753–756
53. Telfah A, Jafar MMAG, Jum'h I, Ahmad MJA, Lambert J, Hergenröder R (2018) Identification of relaxation processes in pure polyethylene oxide (PEO) films by the dielectric permittivity and electric modulus formalisms. *Polym Adv Technol* 29:1974–1987

Publisher's Note Springer Nature remains neutral with regard to jurisdictional claims in published maps and institutional affiliations.